THE JOURNAL OF PHYSICAL CHEMISTRY C

Article

pubs.acs.org/JPCC

Emergence of Multicolor Photoluminescence in $La_{0.67}Sr_{0.33}MnO_3$ Nanoparticles

Anupam Giri,[†] Nirmal Goswami,[†] M. S. Bootharaju,[‡] Paulrajpillai Lourdu Xavier,[‡] Robin John,[‡] Nguyen T. K. Thanh,[§,∥] Thalappil Pradeep,[‡] Barnali Ghosh,[†] A. K. Raychaudhuri,[†] and Samir Kumar Pal[†,*]

[†]Unit for Nano Science and Technology, S. N. Bose National Centre for Basic Sciences, Block JD, Sector III, Salt Lake, Kolkata 700 098, India

[‡]Department of Chemistry, Indian Institute of Technology Madras, Chennai 600 036 India

[§]Department of Physics and Astronomy, University College London, Gower Street, London WC1E 6BT, United Kingdom

[∥]The Davy-Faraday Research Laboratory, The Royal Institution of Great Britain, 21 Albemarle Street, London, W1S 4BS, United Kingdom

Supporting Information

ABSTRACT: Herein, we report the emergence of multicolor photoluminescence in a mixed-valence manganite nanoparticle $La_{0.67}Sr_{0.33}MnO_3$ (LSMO NP) achieved through electronic structural modification of the nanoparticles upon functionalization with a biocompatible organic ligand, sodium tartrate. From UV−vis absorption, X-ray photoelectron spectroscopy (XPS), time-resolved photoluminescence study, and Raman spectroscopic measurements, it is revealed that ligand-to-metal charge transfer transitions from highest occupied molecular orbital (HOMO, centered in tartrate ligand) to lowest unoccupied molecular orbital (LUMO, centered in $Mn^{3+/4+}$ of the NPs), and d−d transitions involving Jahn−Teller sensitive Mn^{3+} ions in the NPs plays the central role behind the origin of multiple photoluminescence from the ligand functionalized LSMO NPs.

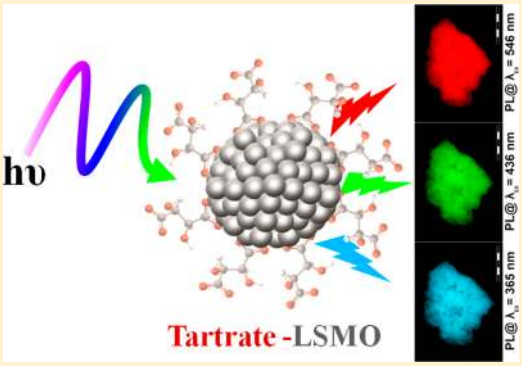

1. INTRODUCTION

The development of nanomaterials with intrinsic photoluminescence are a key focus in nanotechnology for the rational designing of multifunctional nanoparticles and could have profound impact on many research areas ranging from fundamental physics to photoluminescence (PL) devices, catalysis, biological detections, and therapeutics. Several novel nanomaterials have recently been described including quantum dots (QDs),[1−4] magnetic nanoparticles (MNPs),[5,6] magneto-fluorescent nanoparticle,[7−9] and metallic NPs.[10] Their unique optical, magnetic, electronic, and structural properties have addressed a broad spectrum of technological/biological applications.[11−14] Considerable efforts have also been directed toward rational surface modifications to modulate their electronic structure and complicated surface chemistry. However, despite recent advancement, much work still needs to be done to achieve hydrophilic and biocompatible NPs that are luminescent with surface chemistry adaptable to varied technological/biological applications.

In this article, we demonstrate how one can modify the electronic structure of the nanoparticles of functional mixed-valence oxides by making a hybrid with an organic molecule and thereby make the nanoparticles multicolor photoluminescent. The investigation has been done on nanoparticles (NPs) of the perovskite manganite $La_{0.67}Sr_{0.33}MnO_3$ (LSMO), which is known to display a number of exotic properties like colossal magnetoresistance.[15] The functionality of the perovskite manganites arises from mixed valence of Mn ions, which in such system as LSMO have two valence states Mn^{3+} and Mn^{4+}. Presence of Mn^{3+} ions lead to Jahn−Teller distortion around Mn ions, whereas simultaneous presence of Mn^{4+} leads to ferromagnetic double-exchange interactions and metallic behavior.

In recent times, significant efforts have been made to exploit the room temperature ferromagnetism of the perovskite manganite NPs for prospective applications in cancer therapy involving the hyperthermal effect[16] and as dual imaging probes for magnetic resonance imaging and fluorescence microscopy (after tagging an external fluorescent agent).[17] Several experiments have also been focused to solubilize the manganite NPs in aqueous solution by employing some biocompatible macromolecules, still, resulted only in a suspension of the NPs in solution.[17−19] However, in a recent attempt we have functionalized individual manganite NPs with a small

Received: August 30, 2012
Revised: November 7, 2012
Published: November 9, 2012

biocompatible ligand to solubilize them into water and the functionalized NPs shows extremely high colloidal stability.[20]

Herein, we report a new class of multifunctional nanoprobe based on $La_{0.67}Sr_{0.33}MnO_3$ (LSMO) NPs, a mixed-valent manganite where Mn present in two oxidation states, +3 and +4. We have demonstrated the novel optical properties of LSMO NPs upon interaction with sodium tartrate, a dicarboxylate ligand used to solubilized the NPs into water. UV−vis spectroscopic study of the tartrate functionalized LSMO (T−LSMO) NPs reveals that different absorption bands originated from various types of electronic transitions involving ligands−NP interaction. One of the important discovery associated with this work is the observation that the resulting changes on electronic structures (achieved by functionalization with sodium tartrate) can lead to the emergences of multiple color photoluminescence from T−LSMO NPs when it is addressed with different excitation wavelengths, where the respective excitation wavelengths have a direct correlation with the observed UV−vis absorption bands. From X-ray photoelectron spectroscopic (XPS) analysis and time-resolved photoluminescence lifetime measurements, we have acquired additional evidence supporting the proposed mechanism regarding the origin of different optical properties of T−LSMO NPs.

2. EXPERIMENTAL SECTION

Tartaric acid, citric acid, malic acid, sodium hydroxide, metal acetates, 2-amino-purine (2AP), potassium bromide (KBr), and phosphate buffer were obtained from Sigma-Aldrich (USA) and used as received without further purification. 4′,6-Diamidino-2-phenylindole (DAPI), Hoechst (H33258), and ethidium bromide (EtBr) were obtained from Molecular Probes. Organic dye COUMARIN 500 (C500) was obtained from exciton.

We have synthesized the bulk LSMO nanoparticles following a reported procedure where a modified sol−gel technique has been designed especially for the preparation of complex oxide nanoparticles and the reaction mechanism was first given by Shankar et al.[21] The structural and magnetic characterization of the as-prepared nanoparticles has also been described in the reported article.[20]

We have solubilized the as-prepared LSMO NPs into water by using the reactivity of hydroxyl (−OH) and carboxylate (COO^-) groups of tartrate. First, we prepared 6 mL of 0.5 M tartrate solution (pH ∼7) and then 200 mg as-prepared LSMO NPs was added to the solution followed by 6 h of extensive mixing by cyclo-mixer. Finally, the nonfunctionalized bigger sized NPs (as evident from Figure S5 of the Supporting Information, only 5−10% of as-prepared LSMO NPs were in the size range of 2−6 nm, which become solubilized by tartrate ligands) were filtered out (by a syringe driven filter of 0.22 μm diameter) and UV−vis optical absorption of the resulting greenish-yellow filtrate solution was measured.

Next, we increased the pH of the resulting greenish-yellow tartrate−LSMO solution from pH ∼7 to pH ∼12, by dropwise addition of NaOH. The greenish-yellow color of the solution turns to yellowish-brown (indicating conversion of surface Mn^{2+} to Mn^{3+}, as in acidic/neutral pH, Mn^{3+} ions are unstable and tend to disproportionate into Mn^{2+} and Mn^{4+}, whereas it is stabilized by the comproportionation of Mn^{2+} and Mn^{4+} in alkaline conditions[22]) and the resulting solution was heated at 70 °C under vigorous stirring condition for 8 h. After eight hours, the solution became highly fluorescence. Photographs of the resulting solution taken under white light and UV light have been presented in Figure 1. Optical spectra of the Tartrate-LSMO NPs solutions were taken with a Shimadzu Model UV-2450 spectrophotometer using a quartz cuvette of 1 cm path length. The characteristic fluorescence excitation and emission spectra of tartrate−LSMO NPs solution were recorded on a Jobin Yvon Model Fluoromax-3 fluorimeter.

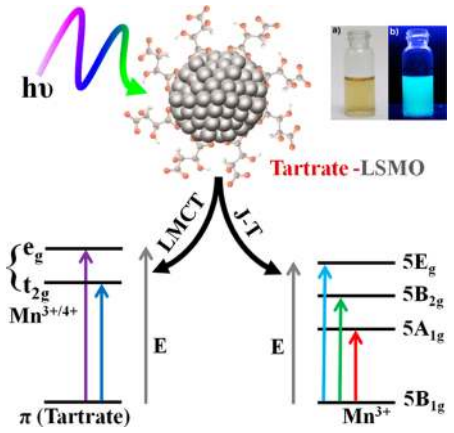

Figure 1. Schematic presentation of the most likely events occurring when a photon hits a tartrate functionalized LSMO NPs (T−LSMO): ligand-to-metal charge transfer transitions from HOMO (centered in tartrate ligand) to LUMO (centered in $Mn^{3+/4+}$ of the NP), and d−d transitions involving Jahn−Teller sensitive Mn^{3+} ions in the NP. Arrows show the transition involved upon excitation by photon of different energy. Insert shows the photographs of T−LSMO NPs under visible light (a) and under UV light (b).

Fluorescence micrographs of as-prepared LSMO and T−LSMO NPs were taken using an Olympus BX51 fluorescence microscope employing 365, 436, and 546 nm excitation wavelengths generated through WBS, WGS, and WUS mirror units, respectively. During the capturing of fluorescence micrographs, in the case of all three excitations (365, 436, and 546 nm), excitation light powers and integration times were kept constant.

TEM samples were prepared by dropping sample stock solutions onto a 300-mesh carbon coated copper grid and dried overnight in air. Particle sizes were determined from micrographs recorded at a magnification of 450 000× using a FEI TecnaiTF-20 field-emission high-resolution transmission electron microscope operating at 200 kV.

XPS measurements were done using an Omicron ESCA Probe spectrometer with polychromatic Al Kα X-rays ($h\upsilon$ = 1486.6 eV). The X-ray power applied was 300 W. The pass energy was 50 eV for survey scans and 20 eV for specific regions. Sample solution was spotted on a molybdenum sample plate and dried in vacuum. The binding energy was calibrated with respect to the adventious C 1s feature at 285.0 eV. Most of the spectra were deconvoluted to their component peaks using the software 6.

A JASCO FTIR-6300 spectrometer was used for the FTIR to confirm the covalent attachment of the tartrate molecules with the LSMO NPs. For FTIR measurements, powdered Tartrate−LSMO samples were mixed with KBr powder and pelletized. The background correction was made by using a reference blank of KBr pellet.

Raman spectroscopic investigations were carried out using a confocal Raman microscope (CRM α300 S) purchased from WITec GmbH, Germany. The spectral acquisition was done in

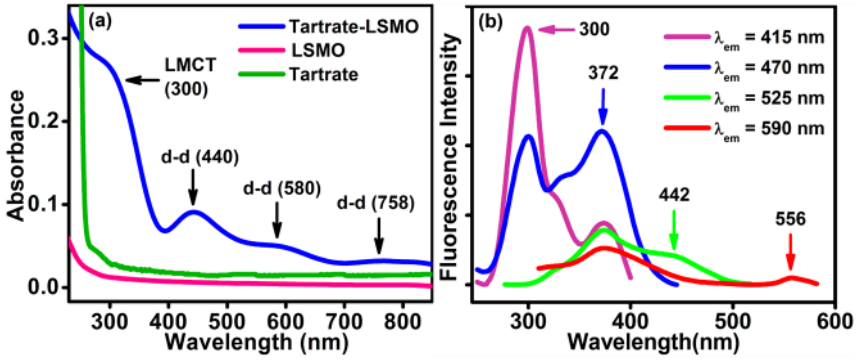

Figure 2. (a) UV−vis absorption spectra of as-prepared LSMO, tartrate, and tartrate−LSMO NPs (in aqueous solution at pH∼7). (b) Photoluminescence excitation spectra of tartrate−LSMO NPs at different emission maximum (shown in part a) of 415, 470, 525, and 590 nm.

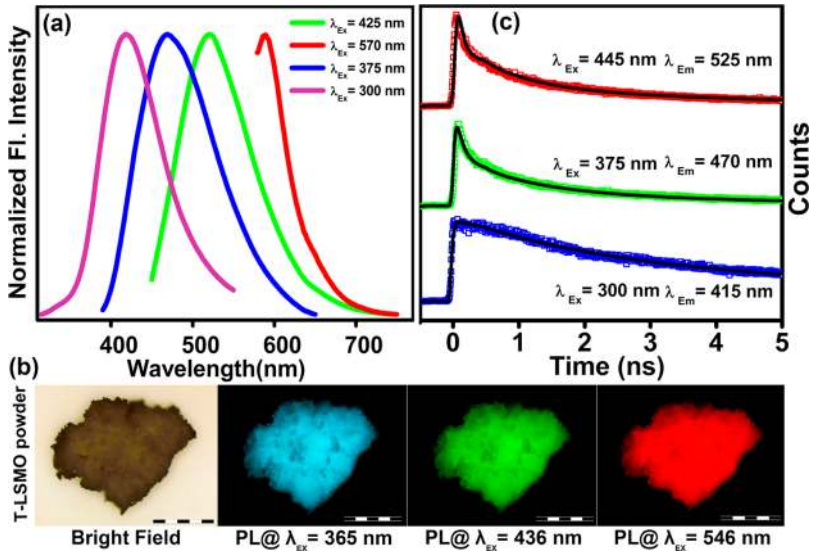

Figure 3. (a) Normalized steady-state photoluminescence spectra collected from tartrate−LSMO NPs with four different excitation wavelengths of 300, 375, 425, and 570 nm at pH ∼7. (b) Fluorescence microscopic images of tartrate−LSMO NP powder under irradiation of white light (bright field) and light of three different wavelengths of 365, 436, and 546 nm. Scale bars in the figure are of 500 μm. (c) Picosecond-resolved photoluminescence decay transients of tartrate−LSMO NPs in water measured at emission wavelengths of 415, 470, and 525 nm upon excitation with laser source of 300, 375, and 445 nm wavelengths, respectively.

a back scattered geometry using a dispersion grating of 600 grooves/mm. The detector used is a peltier cooled charge coupled device, which is maintained at −60 °C. The NPs were excited with a HeNe 532 nm laser source. Each spectrum is an average of 100 hardware spectra, each of which is integrated over 1 s. Raman were measured for LSMO, tartrate, and tartrate−LSMO in solid state, obtained after lyophilizing the corresponding solutions.

Squamous epithelial cells were directly collected from human mouth with proper permission from the volunteer. Prior to cell imaging, the cells were spread on glass slides in presence of PBS (phosphate buffered saline) and NP solution (at a final concentration of 3×10^{-6} M) was added followed by 30 min of incubation at room temperature. After incubation, the cells were washed twice with PBS to remove unbound NPs. Fluorescence micrographs of the cells were taken using an Olympus BX51 fluorescence microscope employing 365, 436, and 546 nm excitation wavelengths generated through WBS, WGS, and WUS mirror units, respectively.

Magnetization curves of Tartrate-LSMO NPs were carried out in a Quantum Design hybrid superconducting quantum interference device-vibrating sample magnetometer (SQUID-VSM) at 5, 50, 100, and 300 K with fields up to 7 T.

Picosecond-resolved fluorescence transients were measured by using commercially available spectrophotometer (Life Spec-ps) from Edinburgh Instruments, UK for 375 nm excitation (80 ps instrument response function, IRF). And for 300 nm excitation, we have used the third harmonic laser beam of 900 nm (0.5 nJ per pulse) using a mode locked Ti-sapphire laser with an 80 MHz repetition rate (Tsunami, Spectra Physics), pumped by a 10 W Millennia (Spectra Physics) followed by a pulse-peaker (rate 8 MHz), and a third harmonic generator (Spectra Physics, model 3980). The third harmonic beam is used for excitation of the sample inside the time-correlated-single-photon-counting (TCSPC) instrument (IRF = 50 ps) and the second harmonic beam is collected for the start pulse. The observed fluorescence transients were fitted by using a nonlinear least-squares fitting procedure to a function

$$(X(t) = \int_0^t E(t')R(t - t')\mathrm{d}t')$$

comprising of convolution of the IRF ($E(t)$) with a sum of exponential

dx.doi.org/10.1021/jp308606a | J. Phys. Chem. C 2012, 116, 25623−25629

$$(R(t) = A + \sum_{i=1}^{N} B_i e^{-t/\tau_i})$$

with pre-exponential factors (B_i), characteristic lifetimes (τ_i), and a background (A). Relative concentration in a multi exponential decay was finally expressed as:

$$c_n = \frac{B_n}{\sum_{i=1}^{N} B_i} \times 100$$

The quality of the curve fitting was evaluated by reduced chi-square and residual data. It has to be noted that with our time-resolved instrument, we can resolve at least one-fourth of the instrument response time constants after the deconvolution of the IRF.

3. RESULTS AND DISCUSSION

Part a of Figure 2 illustrates the UV−vis absorption spectrum of as-prepared LSMO, tartrate, and T−LSMO NPs (at pH ∼7). In the case of T−LSMO, it shows two peaks at 300 and 440 nm, a shoulder descending into lower energies around 580 nm and a broad band at 758 nm. The peak at 300 nm could be assigned to one of the possible high energy charge-transfer, ligand-to-metal charge transfer (LMCT) processes involving tartrate−$Mn^{3+/4+}$ interaction.[23] The other expected LMCT band[23] at around 385 nm has not been observed in the absorption spectrum presumably because the band has been masked by the more intense 300 nm absorption, however, is distinctly visible in the excitation spectrum at around 372 nm (part b of Figure 2). Other bands at 440, 580, and 758 nm are reasonably attributed to d−d transitions of Mn^{3+} in T−LSMO NPs, as the degeneracy of $5E_g$ ground state term of d^4 (Mn^{3+}) high-spin octahedral environment, has been lifted by the Jahn−Teller effect, that ultimately leads to a tentative assignment of the observed bands to the transitions $5B_{1g} \rightarrow 5E_g$, $5B_{1g} \rightarrow 5B_{2g}$, and $5B_{1g} \rightarrow 5A_{1g}$, respectively[24,25] (Figure 1). Any absorption contribution from other metal ions (La and Sr)−tartrate interaction, tartrate ligand or as-prepared LSMO itself, in the assigned peak positions has been nullified from control experiments. Reflection of the UV−vis absorption patterns into the photoluminescence excitation spectra (shown in part b of Figure 2) of the sample has been expected and indeed observed, which further supports the assignment of the electronic excited states those give rise to multiple color photoluminescence.

Part a of Figure 3 displays the normalized photoluminescence spectra of T−LSMO NPs at room temperature. The four distinct emission bands starting from blue to red region (maximum at 418, 470, 520, and 590 nm) of the spectrum corresponding with four distinct excitation wavelengths (300, 375, 425, and 570 nm) are clearly observed. The photoluminescence as shown in part a of Figure 3 may be assigned to originate predominantly from the LMCT [tartrate → $Mn^{3+/4+}$] excited states and ligand field excited states of the metal (Mn^{3+}) d orbitals. Photoluminescence from either an intraligand or metal to ligand charge-transfer (MLCT) excited states are considered unlikely. To represent qualitatively the relationship between emission bands, we have shown the OD normalized PL spectra of T−LSMO NPs in part a of Figure S1 of the Supporting Information. Moreover, to confirm that the lower energy emission spectra are not subsets of high energy emission tail, we have compared the similar excitation wavelength dependent fluorescence emission of a well-known organic dye C500 having one emission maximum centered at 510 nm in water (part c of Figure S1 of the Supporting Information). From the figure, it has been observed that, unlike T−LSMO NPs, despite the change in excitation wavelengths (from 320 to 470 nm), emission maxima of C500 (at around 510 nm) remains same and so its fluorescence decay transients (part d of Figure S1 of the Supporting Information). The observation clearly indicates that the lower energy emission spectra are not subsets of high energy emission tail of T−LSMO NPs.

The above speculation regarding the origin of photoluminescence (PL) is also supported by the pH dependent PL measurements of T−LSMO NPs. As revealed from Figure S2 of the Supporting Information, upon changing the pH of the T−LSMO solution from 12 to 3, its PL intensity quenches significantly, however, almost totally recovered again, by changing the pH from 3 to 12. This phenomenon is consistent with the fact that, in acidic/neutral pH, Mn^{3+} ions are unstable and tend to disproportionate into Mn^{2+} and Mn^{4+}, whereas it is stabilized by the comproportionation of Mn^{2+} and Mn^{4+} in alkaline conditions.[22] Thus, reduction potentials of Mn^{3+}/Mn^{2+} system in acidic and basic solutions ($E^{o}_{Mn3+/Mn2+}$ = 1.51 V at pH 0, whereas $E^{o}_{Mn3+/Mn2+}$ = −0.25 V at pH 14)[26] play a crucial role in understanding the pH dependent PL profile of the studied system. Tartaric acid possesses four protons (two carboxylic acid protons and two hydroxyl protons), which can be liberated depending on pH. However, because of high pK_a (11−12) values of the hydroxyl protons in comparison with the carboxylic protons (pK_{a1} = 2.95 and pK_{a2} = 4.25), they would not liberate at neutral pH and were only available at highly basic pH conditions.[27] Thus, at higher pH, strong co-ordination of tetravalent anionic tartaric acid with Mn^{3+} facilitates both the LMCT and J−T events resulting in a maximization of PL intensity from T−LSMO NPs. However, upon acidification a decrease in pH leads to the protonation of coordinated tartrate molecules along with disproportionation of Mn^{3+} ions and diminishes the overall PL intensity from T−LSMO NPs. Part b of Figure 3 shows the fluorescence microscopic images of T−LSMO powder under irradiation of white light (bright field) and light of different wavelengths (Figure S3 of the Supporting Information shows the fluorescence microscopic images of as-prepared LSMO powder under identical conditions). Multiple color photoluminescence arising specifically from the functionalized NPs (T−LSMO) upon different excitation are clearly evident from the photographs. Photoluminescence quantum yields (QY) of the T−LSMO NPs at pH ∼12, were obtained by using the comparative method of Williams et al.,[28] which involves the use of well characterized standard samples with known QY values. Photoluminescence QY of 1×10^{-2} (for 415 nm PL), 4×10^{-3} (for 470 nm PL), 8×10^{-4} (for 520 nm PL), and 2.4×10^{-4} (for 590 nm PL) were obtained relative to the standards 2-amino-purine (2AP), 4′, 6-diamidino-2-phenylindole (DAPI), Hoechst (H33258), and ethidium bromide (EtBr), respectively.

Further insights into the nature of the photoluminescence can be obtained by analyzing the luminescence lifetime decay transients of T−LSMO NPs in water measured by picosecond-resolved time-correlated single-photon counting (TCSPC) technique. Part c of Figure 3 shows the luminescence lifetime decay transients of the water-soluble NPs at three different emission wavelengths (415, 470, and 525 nm) corresponding with three different laser excitation wavelengths (300, 375, and 445 nm), respectively. Although the origin of 415 and 470 nm

dx.doi.org/10.1021/jp308606a | J. Phys. Chem. C 2012, 116, 25623−25629

Table 1. Fitted Decay Time Constants of T−LSMO NPs from Picosecond Experiments, Values in Parentheses Represent the Relative Weight Percentage of the Time Components

system	excitation wavelength, λ_{ex} (nm)	photoluminescence peak, λ_{em} (nm)	τ_1(ps)	τ_2(ps)	τ_3(ps)	τ_{av}(ns)
T−LSMO NPs	300	415	1846 (45)	7565 (55)		4.77
	375	470	108 (62)	1074 (27)	4982 (11)	0.84
	445	525	56 (69)	737 (20)	4077 (11)	0.64

emission is from the LMCT excited states, luminescence lifetime of 415 nm emission is much longer ($\langle\tau\rangle$ = 4.77 ns) than the 470 nm ($\langle\tau\rangle$ = 0.84 ns) emission (Table 1). Substantial shortening in the luminescence lifetime of 470 nm emission and its close resemblance with the 525 nm emission lifetime ($\langle\tau\rangle$ = 0.64 ns, originates from ligand field excited states of the metal d orbitals) presumably due to enhanced radiative deactivation of the excited state by the close proximity with metal d−d states.[29]

To get supporting evidence regarding the origin of different optical properties of T−LSMO NPs, XPS analysis has been carried out for LSMO NPs, before (as prepared NPs) and after (T−LSMO) functionalization with sodium tartrate (Figure S4 of the Supporting Information). Figure 4 represents the XPS

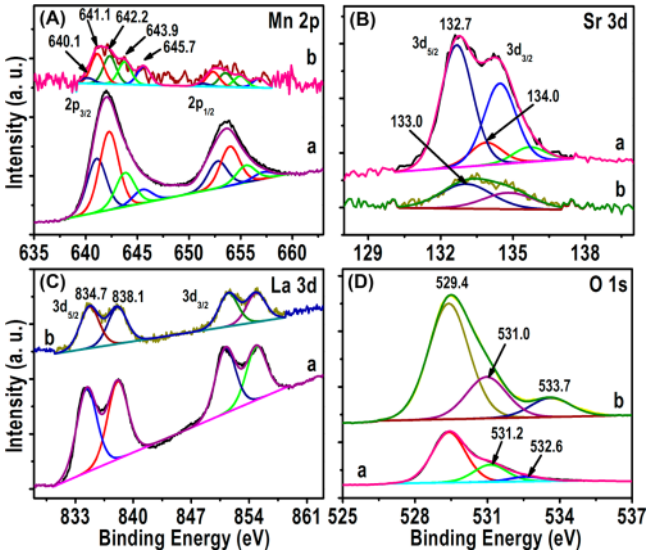

Figure 4. XPS analysis of LSMO NPs before and after functionalization with tartrate (traces a and b, respectively). A, B, C, and D are Mn 2p, Sr 3d, La 3d, and O 1s regions repectively of samples a and b.

data of as-prepared LSMO (traces a) and T−LSMO NPs (traces b). The Mn 2p region is shown in part A of Figure 4. The peaks of Mn $2p_{3/2}$ are observed at 641.1, 642.2, 643.9, and 645.7 eV in both of the samples. The Mn $2p_{3/2}$ features at 641.1 and 642.2 eV are attributed to oxides of Mn^{3+} and Mn^{4+}, respectively.[30] The peak position at 643.9 eV may be due to the manganese in different coordination environment like other metal ions such as La^{3+} and Sr^{2+}.[30] The peak position at 645.7 eV may be due to satellite peak.[31] In the T−LSMO a new feature peaking at 640.1 eV is noticed, which is attributed to Mn^{2+}.[30] The formation of Mn^{2+} could be due to reduction of some of the Mn^{3+}/Mn^{4+} species with tartrate, as reduction of metal ions by tartrate/citrates is expected.[32] The Sr $3d_{5/2}$ peaks at 132.7 and 134.0 eV (part B of Figure 4, trace a) are assigned to Sr^{2+} in the bulk and surface of the NPs, respectively.[33] In the case of T−LSMO, the Sr $3d_{5/2}$ is noticed at 133.0 eV, which is also due to Sr in the divalent (+2) state.[34] The peaks of La $3d_{5/2}$ at 834.7 and 838.1 eV are due to La^{3+} and satellite, respectively (part c of Figure 4) in both of the samples.[35] The O 1s peaks in LSMO NPs at 529.4 and 531.0 eV are due to lattice oxygen O^{2-} associated with Mn and surface oxygen associated hydroxyl ions, respectively.[30] The peak at 532.6 eV is due to the O, which is weakly bound to surface.[36] The peak of O 1s at 533.7 eV in T−LSMO sample is due to carboxylate oxygen from the tartrate.[37] So, from XPS study it is evident that, upon functionalization with tartrate a partial reduction of Mn^{3+} and Mn^{4+} centers in the NPs occur and resulting the formation of Mn^{2+} ions, whereas La^{3+} and Sr^{2+} centers remain unaffected.

It is argued that the change in the valence states of Mn ions will lead to a perturbation of Mn^{3+}−O−Mn^{4+} bond. We do observe the postulated perturbation through Raman spectroscopic investigation on T−LSMO NPs, as prepared LSMO NPs and tartrate. As shown in part a of Figure 5, between the

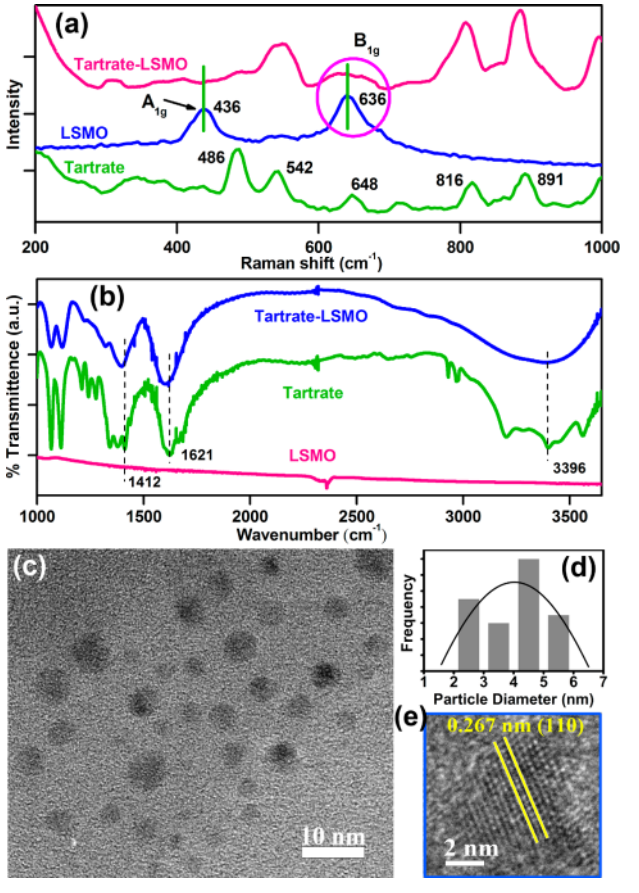

Figure 5. (a) Raman spectra of as-prepared LSMO NPs, tartrate−LSMO NPs and tartrate. (b) FTIR spectra of as prepared LSMO NPs, sodium tartrate, and tartrate functionalized LSMO (tartrate−LSMO) NPs, recorded with a KBr pellet. (c) TEM image of tartrate−LSMO NPs. (d) Size distribution of the NPs in solution. (e) HRTEM image of the crystalline structure of tartrate−LSMO NPs.

dx.doi.org/10.1021/jp308606a | J. Phys. Chem. C 2012, 116, 25623−25629

two characteristic peaks of LSMO NPs at 436 and 636 cm^{-1} (corresponding with A_{1g}-like and B_{1g}-like vibrational modes involving Mn−O stretching vibration modes of MnO_6 unit, respectively),[38] the peak around 436 cm^{-1} completely disappeared and the 636 cm^{-1} peak becomes broadened (possibly due to mixing of tartrate features) after their functionalization with tartrate. Hence, the disappearance of A_{1g}-like stretching vibration mode that represents the extension and compression of Mn−O bond pairs and is directly correlated with Jahn−Teller distortion, provides a strong basis for the changes that occur at the level of MnO_6 octahedra which provides the physical basis for the change in the optical properties of the NPs upon functionalization.

The direct bonding of tartrate ligands to the surface of the LSMO NP has been confirmed by FTIR spectroscopy. Part b of Figure 5 represents the FTIR spectra of as-prepared LSMO NPs, tartrate, and tartrate functionalized LSMO NPs. In case of tartrate, the appearance of two strong bands at 1412 and 1621 cm^{-1} represent the symmetric and asymmetric stretching modes of $-COO^-$ ions (carboxylate), respectively.[39] Upon attachment with the NP surface, these two bands become red-shifted and appear sharply at 1392 and 1596 cm^{-1} respectively and clearly confirm the binding of carboxylate's oxygen with the NPs. Moreover, the significant broadening of the band representing O−H (hydroxyl) stretching vibration mode[40] at 3396 cm^{-1} for tartrate−LSMO also substantiate the involvement of hydroxyl groups during the functionalization process.

As shown in part c of Figure 5, transmission electron microscopy (TEM) revealed that T−LSMO NPs are nearly spherical in shape with an average diameter of around 4 nm (part d of Figure 5). Thus, tartrate ligands only solubilized the small sized particles out of a wide range of particle size from ∼2 to 30 nm in the as-prepared LSMO NPs (Figure S5 of the Supporting Information). The HRTEM image (part e of Figure 5) confirms the crystalline nature of the T−LSMO NPs having interplanar distance of 0.267 nm, which corresponds to the (110) plane of the crystal lattice (as shown in part b of Figure S6 of the Supporting Information, and similar interplanar distance have also been observed in case of as-prepared LSMO NPs). Selected area electron diffraction (SAED) and energy dispersive X-ray (EDAX) pattern of LSMO and T−LSMO NPs also provided supporting evidence (Figures S6 and S7 of the Supporting Information).

Because the tartrate ligand (contains two hydroxyl and two carboxylate groups) is from the class of organic hydroxycarboxylates, we have used two more ligands which are close mimic of tartrate (trisodium citrate and sodium salt of malic acid) and of the same class, for meaningful comparisons with the data obtained from tartrate. It has been observed that both citrate and malate functionalized LSMO NPs exhibit similar UV−vis absorption pattern (part a of Figure 6 and Figure S8 of the Supporting Information, respectively) and excitation wavelength-dependent multiple photoluminescence (in case of citrate−LSMO, parts b and c of Figure 6), which further substantiate the results obtained using tartrate (spectral position of the observed absorption and photoluminescence peaks from these functionalized NPs has been listed in Table S1 of the Supporting Information). Moreover, we have observed the same pH dependent PL profile from citrate−LSMO NPs also (Figure S9 of the Supporting Information). Because of the structural similarity of tartrate and citrate, their pH dependent co-ordination behavior with the NP surface has been expected to be alike. It is revealed that the ligand field of tartrate, citrate and malate can activate the Jahn−Teller (J−T) splitting of Mn^{3+} ions in the NPs and the corresponding d−d transitions along with ligand-to-metal charge transfer transitions (LMCT) plays the crucial role for the emergence of such novel optical properties from LSMO NPs upon functionalization.

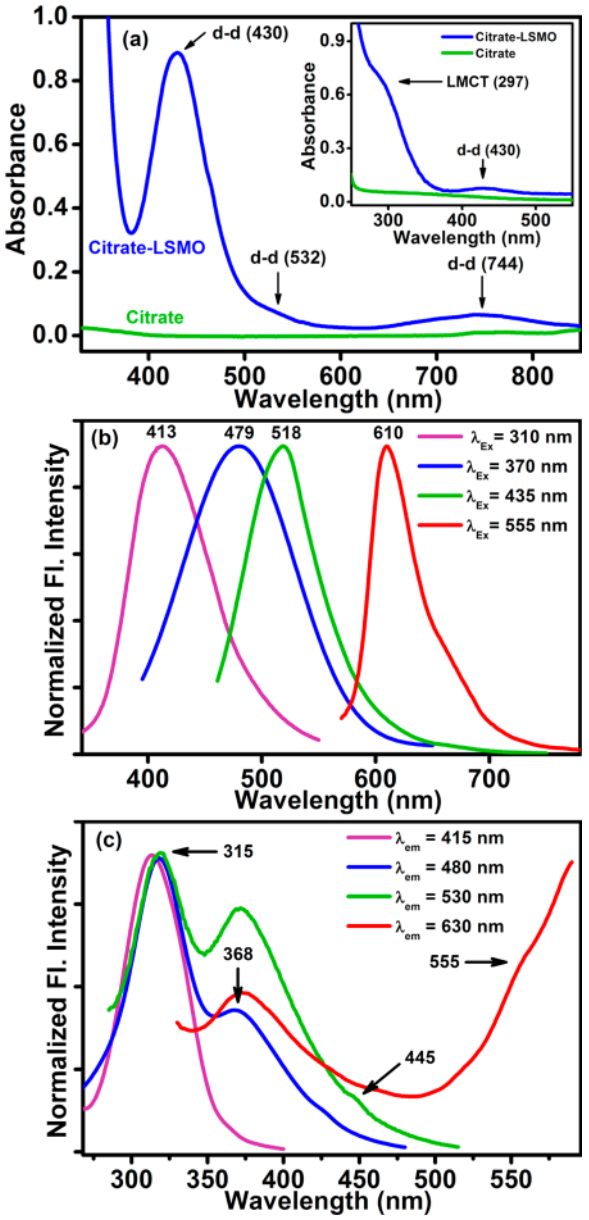

Figure 6. (a) UV−vis absorption spectra of citrate and citrate−LSMO NPs in aqueous solution at pH ∼7. Inset shows the absorption peak (LMCT) at around 300 nm obtained from diluted solution of citrate−LSMO NPs. Although, the entire characteristic peaks/bands are present in case of citrate−LSMO, the observed shift in their positions with respect to T−LSMO NPs could be due to the structural variations of the two ligands. (b) Normalized steady-state photoluminescence spectra collected from citrate−LSMO NPs with four different excitation wavelengths of 310, 370, 435, and 555 nm. (c) Photoluminescence excitation spectra of citrate−LSMO NPs at different emission maximum of 415, 480, 530, and 630 nm.

4. CONCLUSIONS

Within the present studies, we have demonstrated the possibility of electronic structural modifications of manganites NPs (LSMO, and thus the resulting novel optical properties)

dx.doi.org/10.1021/jp308606a | J. Phys. Chem. C 2012, 116, 25623−25629

by charge transfer through functionalization with small organic ligands. The modified electronic structure notably leads to multicolor photoluminescence from the functionalized NPs when excited with different wavelength. We have also explored the mechanistic insight into the origin of multicolor photoluminescence from the T−LSMO NPs. We envision that, given the potentiality of the interaction of Mn^{2+} (easy to convert into Mn^{3+} at high pH), Mn^{3+} (J−T sensitive) and Mn^{4+} toward hydroxycarboxylates (tartrate/citrate) and the consequent origin of novel optical properties, a logical extension of this work would be the functionalization of manganese oxides and various manganese doped nanoparticles including manganese ferrites, ZnO, CdS, and so forth.

■ ASSOCIATED CONTENT

Supporting Information

Detailed characterization of as-prepared LSMO, T−LSMO, citrate−LSMO and malate−LSMO NPs, SQUID measurements and cell imaging study of T−LSMO NPs. This material is available free of charge via the Internet at http://pubs.acs.org.

■ AUTHOR INFORMATION

Corresponding Author

*E-mail: skpal@bose.res.in.

Notes

The authors declare no competing financial interest.

■ ACKNOWLEDGMENTS

The authors would like to acknowledge Mr. Sounik Sarkar and Prof. Anjan Kr. Dasgupta at Department of Biochemistry, University of Calcutta for insightful discussions. A.G. thanks UGC, India, for fellowship. N.G. thanks CSIR, India, for fellowship. We thank DST for financial grants SR/SO/BB-15/2007. The work of A.K.R. and B.G. has been supported by funding from the DST, India as UNANST-II. Equipment support to T.P. was provided by the Nano Mission of DST, India.

■ REFERENCES

(1) Chan, W. C. W.; Nie, S. *Science* **1998**, *281*, 2016−2018.
(2) Taylor, J. R.; Fang, M. M.; Nie, S. *Anal. Chem.* **2000**, *72*, 1979−1986.
(3) Bonadeo, N. H.; Erland, J.; Gammon, D.; Park, D.; Katzer, D. S.; Steel, D. G. *Science* **1998**, *282*, 1473−1476.
(4) Gao, X. H.; Nie, S. M. *Trends. Biotechnol.* **2003**, *21*, 371−373.
(5) Pecorelli, T. A.; Dibrell, M. M.; Li, Z.; Thomas, C. R.; Zink, J. I. *Proc. SPIE* **2010**, *7576*, 75760k.
(6) Gao, F.; Chen, X. Y.; Yin, K. B.; Dong, S.; Ren, Z. F.; Yuan, F.; Yu, T.; Zou, Z. G.; Liu, J. M. *Adv. Mater.* **2007**, *19*, 2889−2892.
(7) Josephson, L.; Kircher, M. F.; Mahmood, U.; Tang, Y.; Weissleder, R. *Bioconjugate Chem.* **2002**, *13*, 554−560.
(8) Kircher, M. F.; Weissleder, R.; Josephson, L. *Bioconjugate Chem.* **2004**, *15*, 242−248.
(9) Cho, N.-H.; Cheong, T.-C.; Min, J. H.; Wu, J. H.; Lee, S. J.; Kim, D.; Yang, J.-S.; Kim, S.; Kim, Y. K.; Seong, S.-Y. *Nat. Nanotechnol.* **2011**, *6*, 675−682.
(10) Verma, P. K.; Giri, A.; Thanh, N. T. K.; Tung, L. D.; Mondal, O.; Pal, M.; Pal, S. K. *J. Mater. Chem.* **2010**, *20*, 3722−3728.
(11) Petros, R. A.; DeSimone, J. M. *Nat. Rev. Drug Discov.* **2010**, *9*, 615−627.
(12) Luo, X.; Morrin, A.; Killard, A. J.; Smyth, M. R. *Electroanalysis* **2006**, *18*, 319−326.
(13) Chen, W. *J. Nanosci. Nanotechnol.* **2008**, *8*, 1019−1051.
(14) Pankhurst, Q. A.; Thanh, N. T. K.; Jones, S. K.; Dobson, J. *J. Phys. D: Appl. Phys.* **2009**, *42*, 224001−224016.
(15) Rao, C. N. R.; Raveau, B. *Colossal Magnetoresistance, Charge Ordering and Related Properties of Manganese Oxides*; World Scientific: Singapore, 1998.
(16) Kim, D. K.; Amin, M. S.; Elborai, S.; Lee, S. H.; Koseoglu, Y.; Zahn, M.; Muhammed, M. *J. Appl. Phys.* **2005**, *97*, 100510.
(17) Kacenka, M.; Kaman, O.; Kotek, J.; Falteisek, L.; Cerny, J.; Jirak, D.; Herynek, V.; Zacharovova, K.; Berkova, Z.; Jendelova, P.; Kupcik, J.; Pollert, E.; Veverka, P.; Lukes, I. *J. Mater. Chem.* **2011**, *21*, 157−164.
(18) Bhayani, K. R.; Kale, S. N.; Arora, S.; Rajagopal, R.; Mamgain, H.; Kaul-Ghanekar, R.; Kundaliya, D. C.; Kulkarni, S. D.; Pasricha, R.; Dhole, S. D.; Ogale, S. B.; Paknikar, K. M. *Nanotechnology* **2007**, *18*, 345101.
(19) Rajagopal, R.; Mona, J.; Kale, S. N.; Bala, T.; Pasricha, R.; Poddar, P.; Sastry, M.; Prasad, B. L. V.; Kundaliya, D. C.; S. B. Ogale, S. B. *Appl. Phys. Lett.* **2006**, *89*, 023107.
(20) Giri, A.; Makhal, A.; Ghosh, B.; Raychaudhuri, A. K.; Pal, S. K. *Nanoscale* **2010**, *2*, 2704−2709.
(21) Shankar, K. S.; Raychaudhuri, A. K. *J. Mater. Res.* **2006**, *21*, 27−33.
(22) Takashima, T.; Hashimoto, K.; Nakamura, R. *J. Am. Chem. Soc.* **2011**, *134*, 1519−1527.
(23) Bodini, M. E.; Willis, L. A.; Riechel, T. L.; Sawyer, D. T. *Inorg. Chem.* **1976**, *15*, 1538−1543.
(24) Matzapetakis, M.; Karligiano, N.; Bino, A.; Dakanali, M.; Raptopoulou, C. P.; Tangoulis, V.; Terzis, A.; Giapintzakis, J.; Salifoglou, A. *Inorg. Chem.* **2000**, *39*, 4044−4051.
(25) Aguado, F.; Rodriguez, F.; Núñez, P. *Phys. Rev. B* **2007**, *76*, 094417.
(26) Miessler, G. L.; Tarr, D. A. *Inorganic Chemistry*, 3rd ed.; Prentice-Hall: Englewood Cliffs, NJ, 2004.
(27) Topolski, A. *Chemical Papers* **2011**, *65*, 389−392.
(28) Williams, A. T. R.; Winfield, S. A.; Miller, J. N. *Analyst* **1983**, *108*, 1067−1071.
(29) Lee, Y. F.; Kirchhoff, J. R. *J. Am. Chem. Soc.* **1994**, *116*, 3599−3600.
(30) Li, F.; Zhang, L. H.; Evans, D. G.; Duan, X. *Colloids Surf., A* **2004**, *244*, 169−177.
(31) Sandell, A.; Jaworowski, A. J. *J. Electron Spectrosc. Relat. Phenom.* **2004**, *135*, 7−14.
(32) Guindy, N. M.; Basily, E. K.; Milad, N. E. *J. Appl. Chem. Biotech.* **1974**, *24*, 407−413.
(33) Cantoni, M.; Petti, D.; Bertacco, R.; Pallecchi, I.; Marre, D.; Colizzi, G.; Filippetti, A.; Fiorentini, V. *Appl. Phys. Lett.* **2010**, *97*, 032115.
(34) Ding, T. Z.; Li, J.; Qi, Q. G.; Ji, B. H.; Liu, J.; Zhang, C. Z. *J. Rare Earth.* **2003**, *21*, 453−457.
(35) Samal, A. K.; Pradeep, T. *J. Phys. Chem. C* **2010**, *114*, 5871−5878.
(36) Zou, G.; You, X.; He, P. *Mater. Lett.* **2008**, *62*, 1785−1788.
(37) Bootharaju, M. S.; Pradeep, T. *J. Phys. Chem. C* **2010**, *114*, 8328−8336.
(38) Liang, S.; Teng, F.; Bulgan, G.; Zhu, Y. *J. Phys. Chem. C* **2007**, *111*, 16742−16749.
(39) Ramakrishnan, V.; Maroor, J. M. T. *Infra. Phys.* **1988**, *28*, 201−204.
(40) Kaneko, N.; Kaneko, M.; Takahashi, H. *Spectrochim. Acta Mol.* **1984**, *40*, 33−42.